The Astrophysical Journal, 853:109 (11pp), 2018 February 1 https://doi.org/10.3847/1538-4357/aa9710
© 2018. The American Astronomical Society. All rights reserved.

A Testable Conspiracy: Simulating Baryonic Effects on Self-interacting Dark Matter Halos

Oliver D. Elbert[1], James S. Bullock[1], Manoj Kaplinghat[1], Shea Garrison-Kimmel[2], Andrew S. Graus[1], and Miguel Rocha[3]
[1] Center for Cosmology, Department of Physics and Astronomy, University of California, Irvine, CA 92697, USA; oelbert@uci.edu
[2] TAPIR, California Institute of Technology, Pasadena, CA 91125, USA
[3] SciTech Analytics, Inc., Santa Cruz, CA 95062, USA
Received 2017 June 16; revised 2017 October 18; accepted 2017 October 27; published 2018 January 26

Abstract

We investigate the response of self-interacting dark matter (SIDM) halos to the growth of galaxy potentials using idealized simulations, with each run in tandem with collisionless cold dark matter (CDM). We find that if the stellar potential strongly dominates in the central parts of a galaxy, then SIDM halos can be as dense as CDM halos on observable scales. For extreme cases, core collapse can occur, leading to SIDM halos that are denser and cuspier than their CDM counterparts. If the stellar potential is not dominant, then SIDM halos retain isothermal cores with densities far below CDM predictions. When a disk is present, the inner SIDM halo becomes more flattened in the disk plane than the CDM halo. These results are in excellent quantitative agreement with the predictions of Kaplinghat et al. We also simulated a cluster halo with a central stellar distribution similar to the brightest central galaxy of the cluster A2667. An SIDM halo simulated with the cross-section over mass $\sigma/m = 0.1$ cm^2 g^{-1} provides a good match to the measured dark matter (DM) density profile, while an adiabatically contracted CDM halo is denser and cuspier. The profile of the same halo simulated with $\sigma/m = 0.5$ cm^2 g^{-1} is not dense enough. Our findings are in agreement with previous results that $\sigma/m \gtrsim 0.1$ cm^2 g^{-1} is disfavored for DM collision velocities above about 1500 km s^{-1}. More generally, the interaction between baryonic potentials and SIDM densities offers new directions for constraining SIDM cross-sections in galaxies where baryons are dynamically important.

Key words: dark matter – galaxies: evolution

1. Introduction

The dark matter (DM) paradigm has been tremendously successful in explaining the large-scale structure of our universe (see, e.g., Planck Collaboration et al. 2016; Rodríguez-Torres et al. 2016), though the precise nature of DM remains unknown. The simplest example of cold dark matter (CDM), consisting of a single, collisionless particle with negligible primordial thermal velocity dispersion, can match the large-scale data remarkably well. Alternatively, DM could be more complex, with nongravitational coupling to standard model particles (e.g., Boehm & Schaeffer 2005; Escudero et al. 2015) and/or new dark sector particles (e.g., Feng et al. 2010a; Khlopov et al. 2010; Lesgourgues et al. 2016); many models of this kind produce observable signatures in astronomical data sets (Mangano et al. 2006; Feng et al. 2009; Cyr-Racine et al. 2016). In this paper, we consider the possibility that DM has strong elastic self-scattering interactions and explore the implications of such interactions on the DM distributions within individual galaxies. We specifically focus on the back-reaction associated with galaxy formation.

Collisional or self-interacting dark matter (SIDM) was first explored in the context of galaxy formation by Spergel & Steinhardt (2000), who argued that SIDM models with the cross-section over mass $\sigma/m \sim 1$ cm^2 g^{-1} should lead to observable constant-density cores in galaxies, which is in agreement with observations at that time. While early estimates suggested that SIDM models of this kind would significantly reduce substructure counts compared to CDM, more recent numerical investigations have shown that the substructure differences are minimal (Vogelsberger et al. 2012; Rocha et al. 2013). However, the original expectation that SIDM halos should have constant-density cores has been demonstrated robustly in cosmological simulations (Davé et al. 2001; Rocha et al. 2013; Zavala et al. 2013).

SIDM cores are generated by energy-exchange interactions, which heat the halo center until it becomes isothermal. The radial extent of this core is set by the requirement that a typical DM particle will experience at least one interaction per Hubble time (Rocha et al. 2013). This implies that larger SIDM cross-sections produce larger isothermal cores. If the cross-section is large enough, then the isothermal region can extend beyond the peak in the halo's velocity dispersion profile; in this case, energy-exchange interactions could extract heat from the core leading to core collapse, which increases the central density (Kochanek & White 2000; Balberg et al. 2002; Colín et al. 2002; Koda & Shapiro 2011; Vogelsberger et al. 2012). However, this effect is muted in cosmological simulations and Elbert et al. (2015) used DM (only) zoom cosmological simulations to show that core collapse behavior sets in only for very large cross-sections $\sigma/m \gtrsim 10$ cm^2 g^{-1}.

The tendency for SIDM models with $\sigma/m \lesssim 10$ cm^2 g^{-1} to produce constant-density cores with lower overall density is of special interest for comparisons to dwarf and low-surface brightness (LSB) galaxies. This is because many of these galaxies are observed to have cores on roughly the scales that are expected in SIDM (Flores & Primack 1994; Moore 1994; de Blok et al. 1996; Salucci & Burkert 2000; de Blok et al. 2001; Swaters et al. 2003; Gentile et al. 2004; Simon et al. 2005; Spekkens et al. 2005; de Blok et al. 2008; Kuzio de Naray et al. 2008; Donato et al. 2009; Oh et al. 2011; Adams et al. 2014), as opposed to the cusps predicted in dissipationless CDM simulations (Dubinski & Carlberg 1991; Navarro et al. 1997). SIDM cores also may provide a natural

explanation for the unexpectedly low densities of local dwarf galaxies (Vogelsberger et al. 2012, 2014; Elbert et al. 2015), which is a problem known as "Too Big to Fail" (TBTF; Boylan-Kolchin et al. 2011, 2012; Ferrero et al. 2012; Garrison-Kimmel et al. 2014; Tollerud et al. 2014; Klypin et al. 2015; Papastergis et al. 2015). There are many in the galaxy formation community who believe these issues may be resolved by baryonic processes, such as supernova feedback (Navarro et al. 1996; Read & Gilmore 2005; Governato et al. 2012; Pontzen & Governato 2012; Di Cintio et al. 2014; Maxwell et al. 2015; Oñorbe et al. 2015; Dutton et al. 2016; Read et al. 2016; Katz et al. 2017), though not all authors necessarily agree (Peñarrubia et al. 2012; Garrison-Kimmel et al. 2013; Pace 2016). Tidal effects have been shown to solve TBTF in satellite galaxies (see e.g., Read et al. 2006; Zolotov et al. 2012; Arraki et al. 2014; Brooks & Zolotov 2014; Del Popolo et al. 2014), but the evidence for TBTF in the local field (Garrison-Kimmel et al. 2014; Kirby et al. 2014) necessitates another solution for these galaxies. This ongoing debate and the lack of DM detections in direct, indirect, and collider searches motivates a thorough exploration of the SIDM hypothesis.

The goal of this paper is to investigate the late-time effects of galaxy formation on SIDM halos, specifically the contraction of these halos due to the gravitational potential of the galaxy. To this end, we use a set of *N*-body simulations similar to those initially used to examine contraction in CDM halos. The work is organized as follows. In Section 2, we briefly describe the properties required of a viable SIDM model, and in Section 3, we sketch the physics of contraction of SIDM halos and motivate our work in this paper. We describe our simulations and analysis in Section 4. We present our results in Section 5, discussing our Milky Way analog halos in Section 5.1 and our elliptical and LSB simulations in Section 5.2, while in Section 5.3, we directly compare our simulations to the analytic model presented in Kaplinghat et al. (2016). Section 6 shows the results of our cluster simulations and compares these with the observations of Newman et al. (2013b). We summarize our results and conclude in Section 7.

2. Properties of Viable SIDM Models

Previous work has placed constraints on the SIDM cross-section over mass across a range of halo masses. Generally, σ/m below 0.1 $\mathrm{cm^2\ g^{-1}}$ have been found to be indistinguishable from CDM models (Rocha et al. 2013). In low-mass galaxies with maximum circular velocity of $V_{\rm max} \simeq 30\ \mathrm{km\ s^{-1}}$, σ/m, values ranging from 0.5 to 10 $\mathrm{cm^2\ g^{-1}}$ alleviate the core-cusp and TBTF (Vogelsberger et al. 2012; Zavala et al. 2013; Elbert et al. 2015; Fry et al. 2015). However, values significantly in excess of 1 $\mathrm{cm^2\ g^{-1}}$ may lead to the efficient tidal stripping of stars in the satellites of the Milky Way and Andromeda (Gnedin & Ostriker 2001; Peñarrubia et al. 2010; Dooley et al. 2016), providing a possible avenue for an upper limit on the cross-section in the future. Recent work by Kaplinghat et al. (2016) showed that SIDM models with cross-sections around 2 $\mathrm{cm^2\ g^{-1}}$ fit the rotation curves of the 12 analyzed dwarf and LSB galaxies well. This work used an analytic model built on arguments discussed previously (Rocha et al. 2013; Kaplinghat et al. 2014) and showed that the analytic model is a good match for the density profiles of halos in DM-only cosmological SIDM simulations. The summary of above constraints is that for collisional velocities of order $100\ \mathrm{km\ s^{-1}}$ or smaller, a σ/m values close to 1 $\mathrm{cm^2\ g^{-1}}$ is favored and is consistent with all existing constraints. A larger sample of rotation curves will reduce uncertainties in the determination of the cross-section on galactic velocity scales.

The DM velocities in galaxy clusters are an order of magnitude larger than in dwarf galaxies, and many techniques have been used to constrain the DM self-interaction cross-section at these velocities. Cluster mergers have been used by many studies to constrain SIDM (see e.g., Randall et al. 2008; Dawson et al. 2012; Kahlhoefer et al. 2014; Massey et al. 2015; Schaller et al. 2015; Kim et al. 2017; Robertson et al. 2017), with typical limits of $\sigma/m \leqslant 1\ \mathrm{cm^2\ g^{-1}}$ on the self-interaction cross-section. However, recent work by Kim et al. (2017) showed that constraints based on the displacement of the stellar and DM centroids are overly stringent, weakening previous constraints. They find that the displacement of the brightest cluster galaxy (BCG) relative to the halo center may be a better observable, possibly allowing σ/m values around 0.1 $\mathrm{cm^2\ g^{-1}}$ to be tested. The Bullet cluster constraint based on the mass loss from the merging subcluster (Markevitch et al. 2004) also needs to be reevaluated using self-consistent SIDM merger simulations and taking into account cosmic variance in the initial conditions. In addition, we also need theoretical refinement to apply these constraints to velocity-dependent cross-sections. Cluster shapes have provided an orthogonal method of investigating self-interaction cross-section on these scales. Core formation in SIDM halos leads to more spherical inner density profiles, so measurements of the ellipticities of cluster halos have been used to constrain σ/m values to below 0.1 $\mathrm{cm^2\ g^{-1}}$ (Miralda-Escudé 2002). However, due to the large scatter in axis ratios, the ability of SIDM halos to retain some triaxiality and the observational methods used to constrain halo shapes, the ellipticity constraints are unlikely to be better than about 1 $\mathrm{cm^2\ g^{-1}}$ for cluster velocities (see Peter et al. 2013 for a detailed discussion).

The most stringent constraint on cluster velocity scale arises from the fact that the measured DM density profiles are in substantial agreement with CDM outside the half-light radii of the BCGs. Within about 10–50 kpc (range of BCG half-light radii), however, the DM density profile is shallower than the CDM expectations (Newman et al. 2013b), as we discuss later. Kaplinghat et al. (2016) used these measurements to show that the preferred cross-section for relative velocities larger than $1000\ \mathrm{km\ s^{-1}}$ is about 0.1 $\mathrm{cm^2\ g^{-1}}$, which is consistent with earlier results from Yoshida et al. (2000). If the inferred shallowness of the density profile is due to AGN feedback or some other baryonic process (e.g., Martizzi et al. 2013), then this value of 0.1 $\mathrm{cm^2\ g^{-1}}$ provides a stringent upper limit on the self-interaction cross-section for velocities in excess of $1000\ \mathrm{km\ s^{-1}}$. This result and the large difference in DM velocities in dwarf galaxies and galaxy clusters demand that viable SIDM models must have a velocity-dependent self-interaction cross-section. The required velocity dependence—from 1 $\mathrm{cm^2\ g^{-1}}$ for velocities below about $100\ \mathrm{km\ s^{-1}}$ to 0.1 $\mathrm{cm^2\ g^{-1}}$ for velocities above $1000\ \mathrm{km\ s^{-1}}$—can be easily accommodated in a variety of particle physics models (Feng et al. 2010b; Loeb & Weiner 2011; Tulin et al. 2013; Boddy et al. 2014, 2016; Cline et al. 2014).

3. Motivation: Contraction of SIDM Halos

Our work on simulating SIDM halos including a baryonic component is important for two specific reasons. First, in

galaxies dominated by baryons there is no systematic evidence for large cores or lowered DM density profiles (e.g., Cappellari et al. 2015). Second, in galaxy clusters the stars dominate the total mass budget within their half-light radii, yet the DM tends to be under-dense compared to predictions. There is a simple analytic model (which we discuss later) that can explain both these observations but it has not been tested against simulations including a stellar component. By testing the accuracy of the analytic model we are able to bolster the case for a velocity-dependent self-interaction cross-section. We also test the possibility of core collapse in systems that have extremely dense baryonic distributions.

In this work, our aim is to test and further elucidate the general physics of how SIDM halos become isothermal in the potential well of the baryons. Because of this, we have chosen to run idealized simulations with disks grown adiabatically. This is complementary to the approach of running full-fledged hydrodynamic simulations that include self-interactions between DM particles. Vogelsberger et al. (2014) and Fry et al. (2015) examine dwarf galaxies ($M_{\rm v} \sim 10^{10}\,M_{\odot}$) using fully self-consistent hydrodynamic simulations and find that observable cores are still formed in these dwarfs in SIDM. Fry et al. (2015) find that the cores in their simulated dwarfs are not substantially different from those formed purely via feedback in their CDM simulations. It is not clear how these results generalize to larger halo masses, where feedback is expected to be less important in driving core formation in CDM halos and halo contraction effects are expected to dominate (e.g., Di Cintio et al. 2014; Dutton et al. 2016; Fiacconi et al. 2016).

The fact that growing baryonic potentials can cause contraction of CDM halos was first investigated analytically by Blumenthal et al. (1986) and Ryden & Gunn (1987), who used an adiabatic invariant approach. They demonstrated that if a baryonic potential grew to dominate the central potential, then the entire dark halo would contract, increasing the central DM density by more than an order of magnitude in plausible cases. Other studies (e.g., Jesseit et al. 2002) ran numerical simulations of isolated DM halos with disk potentials and found the DM density in these halos reproduced analytical predictions. Gnedin et al. (2004) studied baryonic contraction in hydrodynamic cosmological simulations and found that both adiabatic model predictions and isolated simulations produced central densities that were roughly 50% too high in halos where baryons dominate and proposed an alternative model to encapsulate the adiabatic contraction effect.

Though previous work on halo contraction explored collisionless DM, the general results should apply to SIDM as well. The adiabatic contraction occurs at early times when the disk or bulge of a galaxy is forming. These timescales are much shorter than the typical timescale for self-interactions in galaxies, assuming a cross-section around 1 $\rm cm^2\ g^{-1}$. At later times, the self-interaction process will allow the halo to become isothermal, and this process can make the DM density profile shallower, retain the steep density profiles created by adiabatic contraction, or steepen it further in the case of core collapse. As we show later, the outcome depends on the cross-section, the gravitational potential of the baryons and the outer (CDM) DM halo profile.

Feedback could change the density profile of DM for dwarf galaxies, but it is not expected to be important for the baryon-dominated systems we simulate, which are Milky Way size or larger (Di Cintio et al. 2014; Dutton et al. 2016). It is important to note that when the equilibration timescale is short, changes due to feedback need to happen very late in order to prevent the DM from moving toward the equilibrium solution.

Kaplinghat et al. (2014) discussed the response of SIDM halos to the formation of a stellar disk or bulge using analytic equilibrium models. They found that the resultant SIDM core radius and density should be linked closely to the underlying baryonic potential in systems where the baryons are important dynamically. In the limit where the stars dominate the gravitational potential, the DM density profile (in the region where it is isothermal) scales as $\exp(-\Phi_{\star}(r)/\sigma_{v0}^2)$ (Amorisco & Bertin 2010; Kaplinghat et al. 2014) where $\Phi_{\star}$ is the gravitational potential of the stars and σ_{v0} is the 1D central velocity dispersion of DM. Thus, stars and DM are tied together in terms of the density profile and the shape of the DM halo must follow the contours of the stellar gravitational potential. This result emphasizes the need to account for the baryons when exploring SIDM phenomenology in galaxies with significant gas or stellar components.

The goal of this paper is to numerically investigate the effects of baryonic contraction on SIDM halos using a set of isolated *N*-body DM simulations of Milky Way, elliptical, lower sideband (LSB), and cluster analog halos. These simulations are similar in spirit to those first used to test and confirm analytic contraction models in the context of CDM. All of our halos were simulated with fixed SIDM cross-sections of $\sigma/m = 0.5\ \rm cm^2\ g^{-1}$, but we show below that our simulations reproduce the model of Kaplinghat et al. (2016), indicating we can use their model to extend our results to a wide range of cross-sections.

4. Simulations

Because we are primarily interested in isolating the effects of baryonic contraction on SIDM halos, as opposed to modeling a fully realistic treatment of galaxy formation in an SIDM universe, we ignore the effects of halo growth and baryonic feedback in our simulations. To model halos after rapid early accretion has finished, we choose a spherical Navarro et al. (1997) density profile for our initial conditions because it describes the equilibrium state of DM halos well. We may then add the galaxy potential in order to simulate a system without violent starbursts or major mergers. These assumptions and approximations work well for galaxies with quiescent periods greater than SIDM thermalization times ($\lesssim$1 Gyr).

Our code is a modified version of `GADGET-2` (Springel 2005) that allows for the inclusion of hard-sphere scattering between DM particles (Rocha et al. 2013). The simulations consist of a series of 3–50 million particle DM halos, initialized as Navarro et al. (1997) profiles, and run in isolation with and without an analytic galaxy potential. The potentials are grown linearly in time from a mass of zero to a final mass $M_{\rm gal}$ in 1 Gyr at the start of our simulations. We also simulated our Milky Way halo forming the Fiducial Disk after the SIDM core stabilized and found no difference in the DM distribution. The particle initial conditions were generated by the public code `SPHERIC`,[4] which was first introduced in Garrison-Kimmel et al. (2013). To increase our effective resolution we exponentially truncate the outer regions of our initial Navarro–Frank–White (NFW) halos. These truncation radii lie far outside the halo scale radius except in the case of the

[4] https://bitbucket.org/migroch/spheric

Table 1
Summary of Simulated Halos

Name	M_v ($10^{12}\,M_\odot$)	c_v	N_p (10^6)	r_{cut} (kpc)	ϵ (kpc)	Convergence Radius (kpc)	Potential Shape	M_{gal} ($10^{10}\,M_\odot$)	a (kpc)	b (kpc)	h (kpc)
MW	1.0	13	3	230	0.4	0.83	MN Disk	5.0	1.5, 3.0, 6.0	0.3	⋯
LSB	0.2	11.8	10	170	0.19	0.30	MN Disk	0.06	2.2	0.2	⋯
Elliptical	1.8	9.7	10	300	0.37	1.0	Hernquist Sphere	6.2	⋯	⋯	3.0
Cluster	10^3	3	50	500	2	3.4	Hernquist Sphere	210	⋯	⋯	28.5

Note. The first five columns list identifying names and general simulation properties: the halo mass, NFW concentration, particle number, exponential cut-off radius, and force softening. We define M_v following Bryan & Norman (1998), with a virial over-density of $\Delta_v = 97$ with respect to the critical density. The sixth column lists the convergence radius for the SIDM runs, which we set to 0.6 times the Power et al. (2003) radius for CDM, as found in Elbert et al. (2015). The last four columns summarize the properties of the galaxy potentials grown in each case, where M_{gal} is the final galaxy mass and the other shape parameters are defined in Equations (1) and (2). Note that there are three separate disks of varying scale length for the Milky Way runs. We refer to these in the text and figures as "compact," "fiducial," and "extended."

cluster, which we truncate exponentially at 500 kpc in order to resolve the central few kpc of the halo. We have compared our idealized, dark-matter-only halos to analogous cosmological halos presented in Rocha et al. (2013) and found their radial profiles to be in good agreement. This demonstrates that the rapid merging process that forms halos in cosmological simulations does not cause a significant deviation from NFW or isothermal profile.

Table 1 summarizes our simulations, which consist of four characteristic halo/galaxy mass[5] combinations:

1. Milky Way: $M_v = 10^{12}\,M_\odot$ with disks $M_{gal} = 5 \times 10^{10}\,M_\odot$;
2. LSB: $M_v = 2 \times 10^{11}\,M_\odot$ with disk $M_{gal} = 6 \times 10^8\,M_\odot$;
3. Elliptical: $M_v = 1.8 \times 10^{12}\,M_\odot$ with $M_{gal} = 6.2 \times 10^{10}\,M_\odot$; and
4. Cluster: $M_v = 1 \times 10^{15}\,M_\odot$ with $M_{gal} = 2.1 \times 10^{12}\,M_\odot$.

Each of these simulations are run with CDM and SIDM, and also with and without the galaxy potentials for comparison. The Milky Way halo mass simulations include three separate galaxy disk potential runs, each of which has a fixed galaxy mass but a variable scale length (see below). We present 22 simulations in all. All SIDM halos were run with $\sigma/m = 0.5$ cm^2 g^{-1} and used a self-interaction smoothing factor of 25% of the force softening length (Rocha et al. 2013). We also resimulated our cluster halo with $\sigma/m = 0.1$ cm^2 g^{-1}. The force softening and convergence radius (Power et al. 2003; Elbert et al. 2015) of each run are indicated in columns five and six.

For the disk potentials in the LSB and Milky Way runs, we adopt the form of Miyamoto & Nagai (1975, MN hereafter):

$$\Phi_{MN}(R, z) = \frac{-GM_{gal}}{\sqrt{R^2 + (a + \sqrt{b^2 + z^2})^2}}, \quad (1)$$

where a defines a scale length, and b sets a scale height.

Each Milky Way simulation has a fixed scale height of $b = 0.3$ kpc. We explore three scale lengths: $a = 1.5$, 3.0, and 6.0 kpc, which we refer to as "Compact Disk," "Fiducial Disk," and "Extended Disk," respectively. These values[6] roughly span the lower two-sigma to upper one-sigma of disk sizes for $M_{gal} = 5 \times 10^{10}\,M_\odot$ galaxies (Reyes et al. 2011). In particular, the compact disk is extremely dense and was chosen to investigate whether or not core collapse occurs. Our LSB disk mimics a typical LSB from Kuzio de Naray et al. (2008), with $M_{gal} = 6.3 \times 10^8\,M_\odot$, $a = 2.2$ kpc, and $b = 0.2$ kpc.

We use spherical Hernquist (1990) distributions for the elliptical and cluster galaxy runs:

$$\Phi_H(r) = \frac{-GM_{gal}}{(r + h)}. \quad (2)$$

For the elliptical, we adopt $h = 3.0$ kpc and $M_{gal} = 6.2 \times 10^{10}\,M_\odot$, which are motivated by matching the median of bin 28 in Graves et al. (2009). We relate the typical effective radius for galaxies of this size by demanding that the 3D half-light radii are equal: $h = R_e/(1 + \sqrt{2})$. For the central cluster galaxy, we match the results for A2667, as quoted in Newman et al. (2013a), by fitting a Hernquist profile with the same half-light radius to the best-fit dual pseudo-isothermal elliptical (dPIE) profile, which yields $M_{gal} = 2.1 \times 10^{12}\,M_\odot$ and $h = 28.5$ kpc.

Because we do not directly model rapid galaxy formation and feedback in our simulations, we restrict our analysis to the late-time results of contraction, after most of these effects have subsided in massive galaxies. Each simulation was analyzed after reaching dynamical equilibrium, such that the density profile was no longer evolving. This occurred within ∼5 Gyr for all cases except the "compact" SIDM Milky Way, which underwent core collapse and showed a slowly increasing core density until we stopped the simulation after 10 Gyr.

5. Results

5.1. Milky Way Halos

The setup for the Milky Way analog simulations is shown in the left column of Figure 1. The black dotted line shows the circular velocity curve ($V_c(r) = \sqrt{GM(<r)/r}$) for our CDM-only run (equivalent to the initial conditions) and the solid black line shows $V_c(r)$ for SIDM-only run, which is noticeably less dense in the center owing to SIDM core formation (e.g., Rocha et al. 2013). The colored lines show the implied in-plane circular velocities ($\sqrt{r\frac{d\Phi}{dr}|_{z=0}}$) for the imposed Extended, Fiducial, and Compact Disk potentials. These show that the

[5] Our virial mass definition follows Bryan & Norman (1998) for a flat Lambda Cold Dark Matter cosmology with $\Omega_m = 0.27$.

[6] We map the MN disk parameter to quoted exponential disk scale lengths R_d by requiring that the half-mass radii are equal. This implies $a \simeq 1.25R_d$ for the range of parameters we explore.

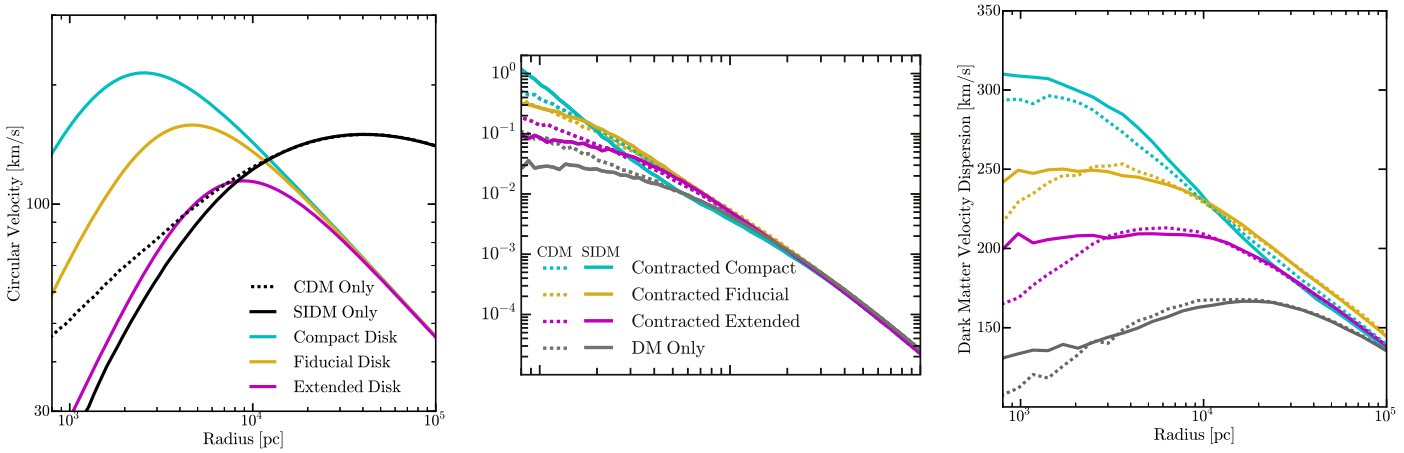

Figure 1. Left: black lines show circular velocity profiles for dark-matter-only Milky Way-size halos (SIDM, solid; CDM, dashed). The colored lines show the circular velocity profiles of three imposed baryonic potentials: Fiducial Disk (yellow), Extended Disk (magenta), and Compact Disk (cyan). Middle: dark matter density profiles without (gray) and with (colored) a response to the grown disk potentials. The lower panel shows the ratio of the SIDM run to CDM run as a function of radius for each set of simulations. Right: velocity dispersion profiles of the same halos, which demonstrate isothermal cores for the SIDM runs, as expected. Note that the relative effect of baryonic contraction is much more substantial in SIDM; the central densities at 600 pc increase by a factor of ∼70 from the noncontracted case to the Compact Disk case in SIDM, compared to only a factor of ∼5 in the CDM case. Interestingly, the Fiducial Disk runs in SIDM and CDM have very similar normalizations, though the SIDM simulation does show a small core developing within ∼800 pc. The Compact Disk, on the other hand, has led to core collapse in the SIDM halo, resulting in a much higher central density than even the contracted CDM halo. Core collapse is expected when the velocity dispersion has a negative gradient within the scattering radius, as is clearly the case for the Compact Disk in the right panel.

disk potential is dominant in our compact and fiducial runs. Our goal is to explore the halo back-reaction to the growth of each of these components.

The middle column of Figure 1 shows the DM density profiles for all simulations. The solid lines correspond to the SIDM model and dotted lines correspond to the CDM model. The gray curves are the dark-matter-only runs, while the colored lines show what happens after the potentials are grown. For reference, the bottom panel plots the ratio of DM density in SIDM to CDM as a function of radius for each set of runs.

As expected, both CDM and SIDM halos contract in response to galaxy potential growth.[7] The relative differences are enlightening. While the dark-matter-only simulations are quite distinct between the cuspy CDM run and the cored SIDM within ∼3 kpc, the DM profiles in the Fiducial Disk runs are almost identical down to the resolving limit. Specifically, the SIDM halo has responded more to the imposed potential than the CDM halo and this has driven the two profiles to a very similar end state. We only begin to see the formation of an SIDM core within ∼1 kpc, which is similar to the Milky Way core size measured in Portail et al. (2017). The Extended Disk runs, which impose a less severe potential, have maintained something closer to the original differences, with SIDM beginning to roll off toward a core within ∼3 kpc, but the differences between the SIDM and CDM are less severe than in the DM-only case (which disagree at 5 kpc). Finally, the Compact Disk has produced a dramatic change: the SIDM halo is now *more dense* than CDM at small radii, with a very cuspy distribution $\rho \sim r^{-2.5}$ at $r \sim 2$ kpc. This is a result of core collapse: the compact disk potential has heated the DM to such an extent that it is now hotter in the core than in the outer part. The SIDM particles are conducting heat outwards, resulting in a loss of core pressure and subsequent mass inflow.

The SIDM phenomenology is clarified in the right panel of Figure 1, which shows the velocity dispersion profile of the DM in each run. The two SIDM simulations with clear constant-density core behavior (DM-only and Extended Disk) are seen to have well-established isothermal velocity distributions at small radii. In these cases, the SIDM halos are hotter in their cores and colder in their outer regions than their CDM counterparts. This is exactly the situation that leads to heat transfer from the outside in. The same effect is seen, though much more mildly, in the Fiducial Disk case. In the Compact Disk runs, even the CDM halo is hotter in the core than in the outer part. Such a declining velocity dispersion profile is subject to outward heat flow in the SIDM simulation, and this drives core collapse.

We show in Section 5.3 that the resultant density profiles are well explained by the analytical predictions presented in Kaplinghat et al. (2014, 2016), with the exception of the Compact Disk. However this is to be expected, given the gravothermal core collapse occurring in the Compact Disk, which violates the assumption of isothermality the model is based on.

Figure 2 displays visualizations of the DM in three pairs of our simulations, with CDM runs shown along the top and SIDM along the bottom. The left row shows the dark-matter-only versions of each simulation. The middle and right rows show resultant DM distributions after the growth of our Fiducial and Compact disks, oriented such that the disks are seen edge-on. These results emphasize that the shapes of the SIDM halos have been altered substantially by the formation of the disk, mirroring the baryonic potential much more closely than the CDM cases within 10 kpc.

5.2. LSB and Elliptical Halos

Figure 3 shows the density profiles and initial rotation curves of our elliptical and LSB halos. In the top left panel, we see that the elliptical halo is baryon-dominated within ∼5 kpc, and consequently the density profiles (bottom left panel) show significant contraction. Again we see minimal difference between the final SIDM and CDM halos, with no SIDM core resolved. This is not surprising, given our results from 5.1;

[7] We have confirmed that our CDM runs generally adhere to the expectations of standard Blumenthal et al. (1986) contraction.

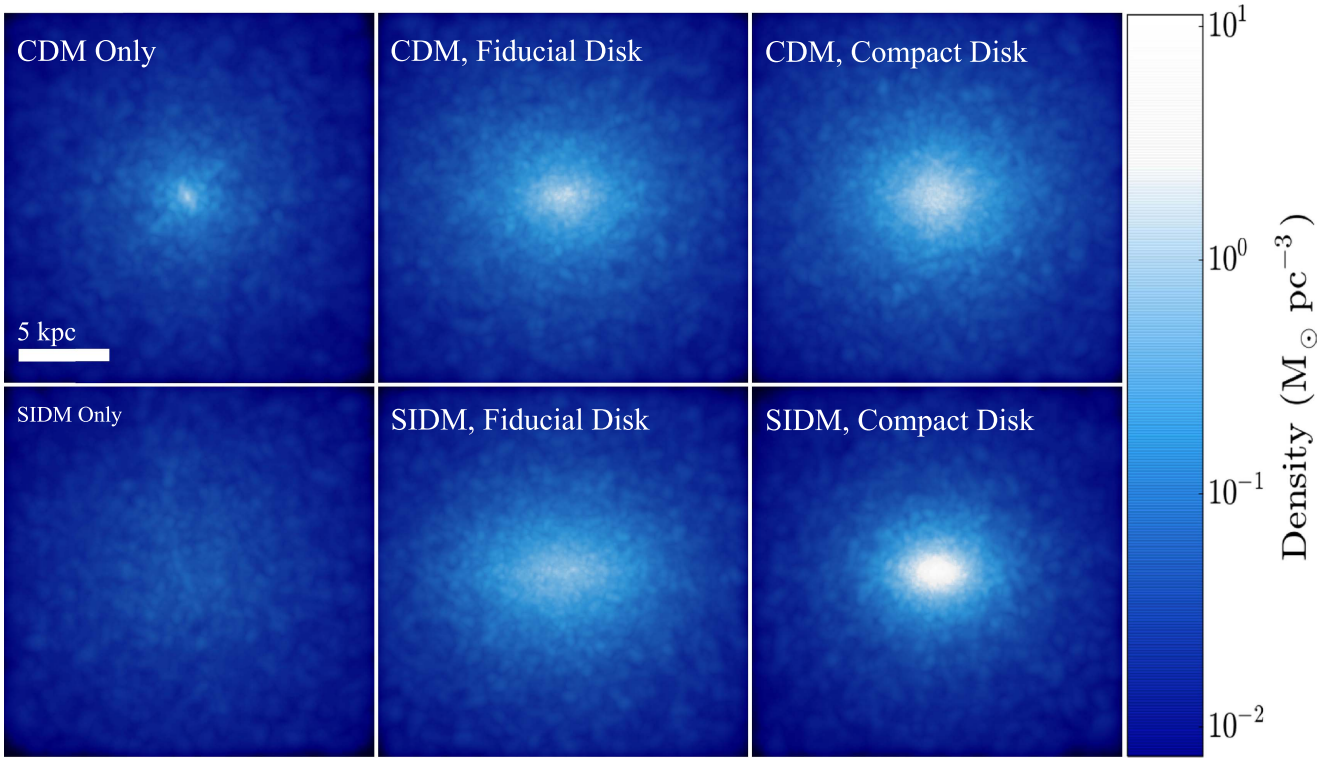

Figure 2. Edge-on visualizations of the dark matter density of an idealized Milky Way-sized halo formed with CDM (top) and SIDM (bottom). Images along the left edge are dark-matter-only runs. The middle panels show the dark matter after the growth of a disk like the Milky Way. The far right panel shows the dark matter after the growth of a compact disk (see Table 1). As expected, the SIDM-only simulation has a much lower central density than the CDM-only case. When a Milky Way-like disk is imposed, both CDM and SIDM halos contract to similar overall central densities, but the SIDM halo tracks the shape of the disk potential more closely than CDM owing to its isothermal velocity distribution. The compact disk case drives core collapse in the SIDM simulation, and thus results in an even higher core density than in the contracted CDM run.

denser galaxies will have greater impacts on their host halos and inhibit SIDM core formation. We also display the total (DM + baryons) density profiles in the bottom left panel of Figure 3, as well as an r^{-2} power-law for comparison. As a result of contraction, both simulations have power-law slopes of $\alpha = -2$ around 3 kpc, and slightly steeper outside this region. This places our simulations in agreement with observations of elliptical galaxies (Gavazzi et al. 2007; Auger et al. 2010). In short, because they are centrally baryon-dominated, predictions for SIDM halos are largely the same as the CDM case for elliptical galaxies.

Our LSB-analog simulations, however, do exhibit differences between CDM and SIDM runs. The right panel of Figure 3 demonstrates that the LSB disk has very little effect on our DM halos; the CDM halo undergoes barely any contraction, and the SIDM halo still displays a central core. This makes sense in light of our previous results that massive and centrally concentrated baryon densities generate the largest impacts on both SIDM and CDM halos. The diffuse nature of low-surface-brightness galaxies implies that their baryons have little effect on the host DM halos. Thus, these systems are the best laboratories to investigate DM self-interaction possibilities.

5.3. Analytic Model

In this section, we compare the results of our simulations to the analytic model presented in Kaplinghat et al. (2016). In this model, the DM is assumed to behave as an isothermal gas within a radius r_1, defined as the radius where particles interact at least once in the age of the system: $\Gamma(r_1)\, t_{\rm age} = 1$ or

$$\rho(r_1)\ (\sigma/m)\ (4/\sqrt{\pi})\sigma_{v0}\, t_{\rm age} = 1. \quad (3)$$

Here, σ/m is the SIDM cross-section per unit mass, σ_{v0} is the radial velocity dispersion in the core and the factor of $4/\sqrt{\pi}$ accounts for the average relative velocity for Maxwellian distribution. $t_{\rm age}$ is the time period over which the self-interactions have been operating. We take this to be the time after the stellar component is fully in place to be consistent with the boundary conditions imposed.

The analytic model we use is spherically symmetric. To apply it to our simulated galaxies, we follow the procedure of Kaplinghat et al. (2014) and construct a new *spherical* mass profile for the baryons $M_{\rm baryon}(r)$ by including all the mass in all the stars within a sphere of radius r. Inside r_1, the SIDM density is set by hydrostatic equilibrium, giving

$$\nabla^2 \ln \rho_{\rm DM}(r) = -\frac{4\pi}{\sigma_{v0}^2} G[\rho_{\rm DM}(r) + \rho_{\rm baryon}(r)], \quad (4)$$

where $\rho_{\rm baryon}$ is the density profile corresponding to the mass profile $M_{\rm baryon}$. As boundary conditions at r_1, the isothermal mass and density profiles (from solving the hydrostatic equation above) are required to match the CDM halo profile after adiabatic contraction (essentially the $z = 0$ CDM profile in our simulations).

In all cases, we find two islands of solutions in the central density—dispersion plane, for the same boundary condition Kaplinghat et al. (2014). We choose the lower density island because it matches the simulated profiles well. Typically, the

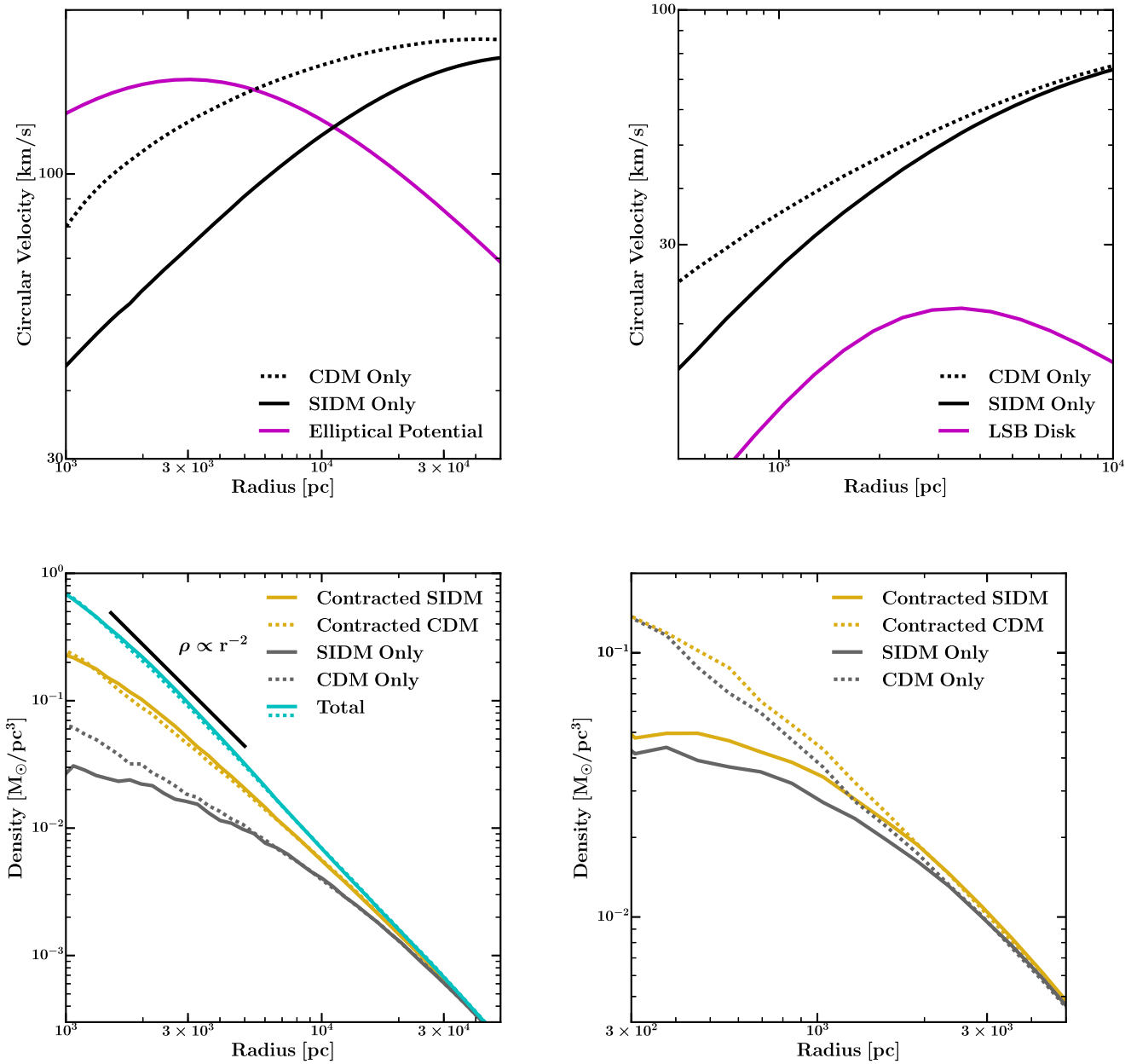

Figure 3. Initial rotation curves and final DM differential density profiles for our elliptical and LSB galaxy simulation, which was simulated in both CDM and SIDM. Left: elliptical simulations. The top panel shows the rotation curves for our CDM and SIDM halos, as well as for the added Hernquist potential, displaying how the halo becomes baryon-dominated within 5 kpc. The bottom panel shows the response of the halos to the added potential; as in the MW disk above, there is very little difference between the two contracted halos. We also include the total (DM plus galaxy potential) density profiles in cyan and an r^{-2} power-law for comparison. Right: LSB simulations. The top panel shows the rotation curves for the initial CDM and SIDM halos along with the central disk potential, which contributes far less to the central mass and density of these halos. The lower panel shows that this relatively shallow baryonic potential has a much smaller impact on the host halo; there is very little difference between the initial and contracted CDM halos. The SIDM halo contracts slightly more, but still retains a core of lower density than the initial CDM halo.

1d central dispersion σ_{v0} values picked out by the two solutions are very close. The value of σ_{v0} value is set by the matching, and it recovers the correct inner dispersion seen in the simulations.

Figure 4 shows circular velocity profiles for our contracted SIDM halos along with the analytic predictions for rotation curves. Here the cyan bands indicate the range of solutions which match $\rho(r_1)$ and $M(r_1)$ within 5%. We chose 5% for two reasons. One, it shows the sensitivity of the inner density profile of SIDM profiles to the matching (boundary) conditions. Two, the simulated SIDM-only and CDM-only halos are not identical and allowing for a small slop in the matching makes us less sensitive to their differences.

The analytic solutions and the simulated halo profiles generally agree well, with the notable exception of the Compact Disk "Milky Way" case. The analytic mass profile for this case is systematically higher, even though the non-trivial shape of the mass profile (see Figure 1) is captured well by the analytic profile. The analytic profile is very sensitive to the value of σ_{v0}. For the Fiducial and Extended disks, the matching correctly infers the SIDM central velocity disperison $\sqrt{3}\,\sigma_{v0}$ to be 250 and 210 km s^{-1} (see Figure 1) and the analytic

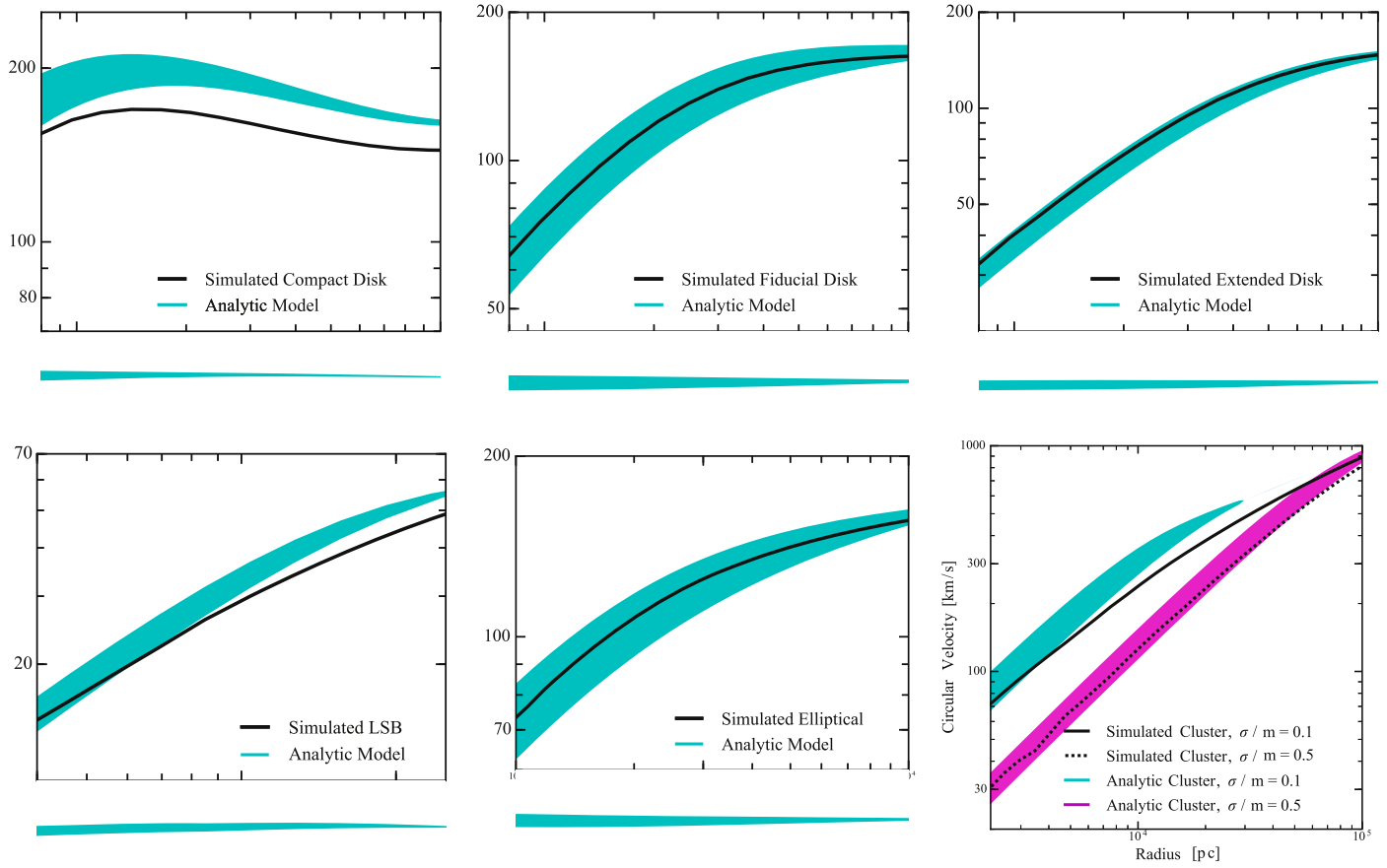

Figure 4. Comparison between circular velocities of our analytic model and simulations. Generally, the analytic model is in agreement with simulations, with the notable exception of the Compact Disk. This is because of the core collapse occurring in the Compact Disk simulation, causing greater central densities than predicted by our model, and leading to higher circular velocities in the halo center.

solution does a good job of describing the simulated mass profiles. For the Compact disk case, the inferred velocity dispersion is close to 290 km s^{-1}. However, in the Compact disk simulation, the velocity dispersion rises this high only within about 2 kpc, while r_1 is about 14 kpc. As Figure 1 shows, the dispersion profile for the Compact disk case is increasing toward the center due to core collapse (see Section 5.1), so the mismatch between the simulated profile and the analytic model is not surprising.

Given the overall consistency of the analytic model (equilibrium) predictions with our simulated halo profiles when core collapse is not seen, we are confident that the Kaplinghat et al. (2016) model predicts the SIDM halos in realistic galaxies and clusters well.

6. Cluster Limits

We also simulate an analog of Abell cluster 2667. Our setup is described in the bottom row of Table 1. The virial mass and concentration of the initial NFW halo match the observations of Newman et al. (2013a), however they model the density of the BCG as a dPIE profile:

$$\rho = \frac{\rho_0}{1 + r^2/(r_{\rm core}^2)(1 + r^2/r_{\rm cut}^2)}$$

In order to model this in our simulations we use a Hernquist (1990) sphere with the same half-mass–radius as the measured profile, and use a least-squares fitting method to obtain a best-fit total mass. This is necessary because dPIE profiles exhibit central cores, while Hernquist profiles have central $1/r$ cusps, so a Hernquist distribution with the same mass and half-mass–radius as a dPIE distribution will be less dense at all radii outside of the core radius and over dense at inner regions, significantly impacting the contraction effect we wish to investigate. The fact that we are using a cuspy profile in our simulations may exaggerate any contraction that occurs in our halos, but both the observed dPIE and our Hernquist profiles are dominant over the DM halo in the central regions, so contraction will occur in either scenario. We grow the central potential over the course of 2 Gyr, and allow the halo to evolve for 3 Gyr after this, running for 5 Gyr total.

Figure 5 shows the density profiles of our simulations; uncontracted densities are plotted as black dashed lines, while the contracted halos are solid black. We also include a vertical arrow to indicate the smallest converged radius of our simulations, as defined in Elbert et al. (2015). We plot the inferred cored NFW DM density profile measured by Newman et al. (2013b) as a cyan band, though we note that the generalized NFW fits Newman et al. (2013b) reported are not significantly different. Finally, the effective density of the BCG Hernquist profile is shown in magenta. The leftmost figure displays our CDM simulations. Even before contraction, the initial NFW profile is too centrally dense to match observations by a factor of ∼1.5 at the limits of our resolution. Adiabatic contraction increases the density by another factor of 1.5, further worsening this discrepancy. If instead we assume the

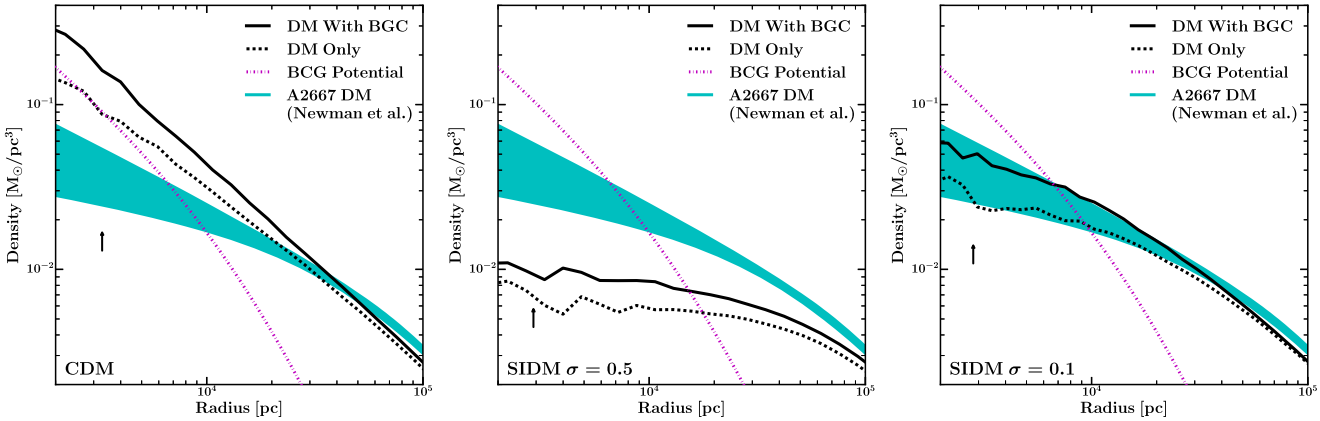

Figure 5. Density profiles for our simulations of cluster Abell 2667, along with the inferred dark matter density profile from Newman et al. (2013b). Even before contraction, our CDM halo (left) is too dense and the contracted SIDM profile with $\sigma/m = 0.5$ cm^2 g^{-1} (center) is not dense enough to reproduce the observed density profile. Our contracted SIDM halo with $\sigma/m = 0.1$ cm^2 g^{-1} (right), however, matches the observed density of Abell 2667 well, and is in agreement with the predictions of Kaplinghat et al. (2016).

DM is self-interacting with a cross-section of 0.5 cm^2 g^{-1}, then we obtain the densities in the center plot. In this case, we see that such a cross-section results in a halo that is under-dense by more than a factor of 3 in its center, and still below the observed limits at 100 kpc in our SIDM-only simulation. While baryonic contraction does increase the DM density, it is not nearly strong enough to completely alleviate the problem. Indeed, over most of our resolved region the contracted halo is only 20%–30% higher than the SIDM-only simulation.

This result may seem surprising at first given that the baryons are important in the center in terms of their dynamical mass. However, the key point is that the DM halo is so massive that its velocity dispersion dwarfs the stellar potential. In this respect, the contraction of the SIDM halo is different from the adiabatic contraction of CDM halos; applying the Blumenthal et al. (1986) adiabatic contraction formula would result in a halo profile much denser than the simulated result. The isothermal equilibrium solution, on the other hand, is a good match to the simulated halo profile.

We also simulate Abell 2667 with a cross-section of 0.1 cm^2 g^{-1}; our results are plotted in the right panel of Figure 5. In the SIDM-only case, the density is near the lower limits of the Newman et al. (2013b) data. After contraction has been accounted for, however, 0.1 cm^2 g^{-1} is consistent with observations, bordering the upper limits of the Newman et al. (2013b) measurement, and we estimate that a cross-section of 0.2 cm^2 g^{-1} will border the lower limits, though a central dPIE galaxy would cause less contraction, making a 0.2 cm^2 g^{-1} cross-section less viable. Our estimates are in agreement with the results of Kaplinghat et al. (2016), who find cross-sections of $0.1 - 0.2$ cm^2 g^{-1} (assuming $t_{\rm age} = 5$ Gyr) by fitting to the Newman et al. (2013b) data using the analytic model (described previously). This implies that an SIDM model with a cross-section that falls from about 1 cm^2 g^{-1} on dwarf galaxy scales to about 0.1 cm^2 g^{-1} on cluster scales can resolve the small-scale puzzles (Zavala et al. 2013; Vogelsberger et al. 2014; Elbert et al. 2015; Kaplinghat et al. 2016), while also matching density profile constraints in clusters.

The Hernquist profile was chosen to have the same half-light radius; however, in detail there are differences especially in the inner parts. It is reasonable to expect that these differences will be reflected in the SIDM density profile for cross-sections around 0.1 cm^2 g^{-1}. To test for the effect of the stellar profile, we used the analytic model to predict the SIDM profile using the dPIE stellar profile rather than Hernquist. As expected, we found no significant differences when the cross-section was set to 0.5 cm^2 g^{-1}. For 0.1 cm^2 g^{-1}, the dPIE profile showed more contraction by about 25% at 1 kpc. These differences are smaller than those when the cross-section is increased by a factor of 2, which provides a guideline to the effect this systematic has on the inferred cross-section. Regardless of the profile shape, a cross-section as large as 0.5 cm^2 g^{-1} cannot fit the inferred density profile for Abell 2667 by Newman et al. (2013b).

7. Conclusions

In this work, we have investigated the combined effects of baryonic gravitational potentials and DM self-interactions on DM halos using idealized simulations of DM halos with galactic potentials. By simulating halos of various sizes with many different potentials we have found the following:

1. SIDM halo shapes are not inherently more resilient to effects from baryons than their CDM counterparts. For a Milky Way halo hosting a Milky Way analog disk, the SIDM halo is more compact along the disk axis than its CDM equivalent in agreement with the prediction of Kaplinghat et al. (2014). For an elliptical galaxy, whose stellar potential is markedly more spherical, we expect the SIDM halo to be correspondingly more spherical.
2. Halos that host substantial baryonic populations display few differences in spherically averaged density profiles between CDM and SIDM models on observable scales. Even extended baryon populations can contract halos with respect to SIDM-only simulations, though these systems retain potentially observable constant-density cores and are less dense than CDM. In extreme cases, we find that potentials from dense baryonic structure can cause SIDM halos to core collapse and become denser than their CDM counterparts.
3. Halos that host concentrated stellar populations may display few differences in spherically averaged density profiles between CDM and SIDM models on observable scales. Even extended stellar populations can contract halos with respect to SIDM-only simulations, though these systems retain potentially observable constant-density

cores and are less dense than CDM. In extreme cases, we find that potentials from dense baryonic structure can cause SIDM halos to core collapse and become denser than their CDM counterparts.

4. The densities of our contracted halos are in good agreement with the analytical predictions in Kaplinghat et al. (2014, 2016), with the exception of the core-collapsing Compact Disk because it no longer obeys the isothermal assumption of the model. In particular, we show that the spherically averaged density profiles are well approximated by the simple model in Kaplinghat et al. (2016), which has an isothermal core and an undisturbed CDM outer profile.
5. We simulated a cluster halo for 3 Gyr after the BCG was fully in place to test against the mass measurements for A2667 Newman et al. (2013b). Our simulated CDM halo was denser than the observed central profile for A2667. On the other hand, SIDM with $\sigma/m \simeq 0.5$ cm^2 g^{-1} was too low in density compared to the measurements. The choice of $\sigma/m \simeq 0.1$ cm^2 g^{-1} was in much better agreement with the measured normalization (and inner slope) of the A2667 density profile. Larger values like $\sigma/m \simeq 0.5$ cm^2 g^{-1} are ruled out, even allowing for a factor of 2 uncertainty in the age of the halo. These conclusions are in substantial agreement with the detailed analysis of 7 clusters (Newman et al. 2013b) by Kaplinghat et al. (2016), which found a average value of $\sigma/m \simeq 0.1$ cm^2 g^{-1} on cluster velocity scales for an assumed age of 5 Gyr.

Based on these results, an ideal scale to investigate possible DM self-interactions appears to be the dwarf galaxy scale with halo masses $10^{10-11}\,M_\odot$ scale, as they will have the largest interaction cross-sections and the least contracted halos. However, these are precisely the halos expected to be most vulnerable to stellar feedback (Governato et al. 2012; Pontzen & Governato 2012; Di Cintio et al. 2014; Oñorbe et al. 2015). Ongoing work (Vogelsberger et al. 2014; Fry et al. 2015; V. Robles et al. 2018, in preparation) is investigating the effects of feedback on the SIDM halos and their results suggest that dwarfs with stellar masses $M_\star \lesssim 10^6\,M_\odot$ will have density profiles indistinguishable from the predictions of the DM-only simulations. This suggests that the faintest dwarf spheroidals provide excellent laboratories constraining SIDM models.

For halo masses much larger than $10^{11}\,M_\odot$ that host a large stellar disk or bulge, as the inner halo becomes isothermal the SIDM halo retains the high densities created by adiabatic contraction following the formation of the disk. Thus, in Milky Way-sized halos the CDM and SIDM halos densities are very similar beyond about a kpc, in marked contrast to the dark-matter-only predictions. As predicted by Kaplinghat et al. (2014), the self-interactions also force the SIDM halo to be more compact along the stellar disk axis. We find that the SIDM halo in the inner region of Milky Way analogs is more compact along the galactic disk axis than the CDM halo. Thus, it may be possible to use the shape of the DM halo in the inner regions of large spiral galaxies to provide a sharp test of the SIDM paradigm.

The predictive cross-talk between the DM and baryons in the SIDM models leads to a large diversity of halo profiles and halo shapes. This cross-talk is purely gravitational and the result of the DM becoming isothermal in the inner parts of the halos. This is fully explained by simple equilibrium models. The prospects for using these concrete predictions of the SIDM paradigm to rule in or rule out SIDM in the near future are excellent.

The authors thank Michael Boylan-Kolchin and Hai-Bo Yu for valuable discussions. O.D.E., A.S.G., and J.S.B. were supported by the National Science Foundation (grants PHY-1520921, AST-1518291, and AST-1009973) and by NASA through *HST* (GO-13343) awarded by the Space Telescope Science Institute (STScI), which is operated by the Association of Universities for Research in Astronomy (AURA), Inc., under NASA contract NAS5-26555. M.K. is supported by NSF grant PHY-1620638. Support for S.G.K. was provided by NASA through Einstein Postdoctoral Fellowship grant number PF5-160136 awarded by the *Chandra* X-ray Center, which is operated by the Smithsonian Astrophysical Observatory for NASA under contract NAS8-03060.

This work also made use of `Astropy`, a community-developed core Python package for Astronomy (Astropy Collaboration et al. 2013), `matplotlib` (Hunter 2007), `numpy` (van der Walt et al. 2011), `scipy` (Jones et al. 2001), `ipython` (Perez & Granger 2007), and NASA's Astrophysics Data System. This work also made use of the EXtreme Science and Engineering Discovery Environment (XSEDE; Towns et al. 2014).

References

Adams, J. J., Simon, J. D., Fabricius, M. H., et al. 2014, ApJ, 789, 63
Amorisco, N. C., & Bertin, G. 2010, A&A, 519, A47
Arraki, K. S., Klypin, A., More, S., & Trujillo-Gomez, S. 2014, MNRAS, 438, 1466
Astropy Collaboration, Robitaille, T. P., Tollerud, E. J., et al. 2013, A&A, 558, A33
Auger, M. W., Treu, T., Bolton, A. S., et al. 2010, ApJ, 724, 511
Balberg, S., Shapiro, S. L., & Inagaki, S. 2002, ApJ, 568, 475
Blumenthal, G. R., Faber, S. M., Flores, R., & Primack, J. R. 1986, ApJ, 301, 27
Boddy, K. K., Feng, J. L., Kaplinghat, M., & Tait, T. M. P. 2014, PhRvD, 89, 115017
Boddy, K. K., Kaplinghat, M., Kwa, A., & Peter, A. H. G. 2016, PhRvD, 94, 123017
Boehm, C., & Schaeffer, R. 2005, A&A, 438, 419
Boylan-Kolchin, M., Bullock, J. S., & Kaplinghat, M. 2011, MNRAS, 415, L40
Boylan-Kolchin, M., Bullock, J. S., & Kaplinghat, M. 2012, MNRAS, 422, 1203
Brooks, A. M., & Zolotov, A. 2014, ApJ, 786, 87
Bryan, G. L., & Norman, M. L. 1998, ApJ, 495, 80
Cappellari, M., Romanowsky, A. J., Brodie, J. P., et al. 2015, ApJL, 804, L21
Cline, J. M., Liu, Z., Moore, G. D., & Xue, W. 2014, PhRvD, 90, 015023
Colín, P., Avila-Reese, V., Valenzuela, O., & Firmani, C. 2002, ApJ, 581, 777
Cyr-Racine, F.-Y., Sigurdson, K., Zavala, J., et al. 2016, PhRvD, 93, 123527
Davé, R., Spergel, D. N., Steinhardt, P. J., & Wandelt, B. D. 2001, ApJ, 547, 574
Dawson, W. A., Wittman, D., Jee, M. J., et al. 2012, ApJL, 747, L42
de Blok, W. J. G., McGaugh, S. S., Bosma, A., & Rubin, V. C. 2001, ApJL, 552, L23
de Blok, W. J. G., McGaugh, S. S., & van der Hulst, J. M. 1996, MNRAS, 283, 18
de Blok, W. J. G., Walter, F., Brinks, E., et al. 2008, AJ, 136, 2648
Del Popolo, A., Lima, J. A. S., Fabris, J. C., & Rodrigues, D. C. 2014, JCAP, 4, 021
Di Cintio, A., Brook, C. B., Dutton, A. A., et al. 2014, MNRAS, 441, 2986
Donato, F., Gentile, G., Salucci, P., et al. 2009, MNRAS, 397, 1169
Dooley, G. A., Peter, A. H. G., Vogelsberger, M., Zavala, J., & Frebel, A. 2016, MNRAS, 461, 710
Dubinski, J., & Carlberg, R. G. 1991, ApJ, 378, 496
Dutton, A. A., Macciò, A. V., Dekel, A., et al. 2016, MNRAS, 461, 2658

Elbert, O. D., Bullock, J. S., Garrison-Kimmel, S., et al. 2015, MNRAS, 453, 29
Escudero, M., Mena, O., Vincent, A. C., Wilkinson, R. J., & Bœhm, C. 2015, JCAP, 9, 034
Feng, J. L., Kaplinghat, M., Tu, H., & Yu, H.-B. 2009, JCAP, 7, 004
Feng, J. L., Kaplinghat, M., & Yu, H.-B. 2010a, PhRvD, 82, 083525
Feng, J. L., Kaplinghat, M., & Yu, H.-B. 2010b, PhRvL, 104, 151301
Ferrero, I., Abadi, M. G., Navarro, J. F., Sales, L. V., & Gurovich, S. 2012, MNRAS, 425, 2817
Fiacconi, D., Madau, P., Potter, D., & Stadel, J. 2016, ApJ, 824, 144
Flores, R. A., & Primack, J. R. 1994, ApJL, 427, L1
Fry, A. B., Governato, F., Pontzen, A., et al. 2015, MNRAS, 452, 1468
Garrison-Kimmel, S., Boylan-Kolchin, M., Bullock, J. S., & Kirby, E. N. 2014, MNRAS, 444, 222
Garrison-Kimmel, S., Rocha, M., Boylan-Kolchin, M., Bullock, J. S., & Lally, J. 2013, MNRAS, 433, 3539
Gavazzi, R., Treu, T., Rhodes, J. D., et al. 2007, ApJ, 667, 176
Gentile, G., Salucci, P., Klein, U., Vergani, D., & Kalberla, P. 2004, MNRAS, 351, 903
Gnedin, O. Y., Kravtsov, A. V., Klypin, A. A., & Nagai, D. 2004, ApJ, 616, 16
Gnedin, O. Y., & Ostriker, J. P. 2001, ApJ, 561, 61
Governato, F., Zolotov, A., Pontzen, A., et al. 2012, MNRAS, 422, 1231
Graves, G. J., Faber, S. M., & Schiavon, R. P. 2009, ApJ, 698, 1590
Hernquist, L. 1990, ApJ, 356, 359
Hunter, J. D. 2007, CSE, 9, 90
Jesseit, R., Naab, T., & Burkert, A. 2002, ApJL, 571, L89
Jones, E., Oliphant, T., Peterson, P., et al. 2001, Open Source Scientific Tools for Python
Kahlhoefer, F., Schmidt-Hoberg, K., Frandsen, M. T., & Sarkar, S. 2014, MNRAS, 437, 2865
Kaplinghat, M., Keeley, R. E., Linden, T., & Yu, H.-B. 2014, PhRvL, 113, 021302
Kaplinghat, M., Tulin, S., & Yu, H.-B. 2016, PhRvL, 116, 041302
Katz, H., Lelli, F., McGaugh, S. S., et al. 2017, MNRAS, 466, 1648
Khlopov, M. Y., Mayorov, A. G., & Soldatov, E. Y. 2010, IJMPD, 19, 1385
Kim, S. Y., Peter, A. H. G., & Wittman, D. 2017, MNRAS, 469, 1414
Kirby, E. N., Bullock, J. S., Boylan-Kolchin, M., Kaplinghat, M., & Cohen, J. G. 2014, MNRAS, 439, 1015
Klypin, A., Karachentsev, I., Makarov, D., & Nasonova, O. 2015, MNRAS, 454, 1798
Kochanek, C. S., & White, M. 2000, ApJ, 543, 514
Koda, J., & Shapiro, P. R. 2011, MNRAS, 415, 1125
Kuzio de Naray, R., McGaugh, S. S., & de Blok, W. J. G. 2008, ApJ, 676, 920
Lesgourgues, J., Marques-Tavares, G., & Schmaltz, M. 2016, JCAP, 2, 037
Loeb, A., & Weiner, N. 2011, PhRvL, 106, 171302
Mangano, G., Melchiorri, A., Serra, P., Cooray, A., & Kamionkowski, M. 2006, PhRvD, 74, 043517
Markevitch, M., Gonzalez, A. H., Clowe, D., et al. 2004, ApJ, 606, 819
Martizzi, D., Teyssier, R., & Moore, B. 2013, MNRAS, 432, 1947
Massey, R., Williams, L., Smit, R., et al. 2015, MNRAS, 449, 3393
Maxwell, A. J., Wadsley, J., & Couchman, H. M. P. 2015, ApJ, 806, 229
Miralda-Escudé, J. 2002, ApJ, 564, 60
Miyamoto, M., & Nagai, R. 1975, PASJ, 27, 533
Moore, B. 1994, Natur, 370, 629
Navarro, J. F., Eke, V. R., & Frenk, C. S. 1996, MNRAS, 283, L72
Navarro, J. F., Frenk, C. S., & White, S. D. M. 1997, ApJ, 490, 493
Newman, A. B., Treu, T., Ellis, R. S., et al. 2013a, ApJ, 765, 24
Newman, A. B., Treu, T., Ellis, R. S., & Sand, D. J. 2013b, ApJ, 765, 25
Oh, S.-H., de Blok, W. J. G., Brinks, E., Walter, F., & Kennicutt, R. C., Jr. 2011, AJ, 141, 193
Oñorbe, J., Boylan-Kolchin, M., Bullock, J. S., et al. 2015, MNRAS, 454, 2092
Pace, A. B. 2016, arXiv:1605.05326
Papastergis, E., Giovanelli, R., Haynes, M. P., & Shankar, F. 2015, A&A, 574, A113
Peñarrubia, J., Benson, A. J., Walker, M. G., et al. 2010, MNRAS, 406, 1290
Peñarrubia, J., Pontzen, A., Walker, M. G., & Koposov, S. E. 2012, ApJL, 759, L42
Perez, F., & Granger, B. E. 2007, CSE, 9, 21
Peter, A. H. G., Rocha, M., Bullock, J. S., & Kaplinghat, M. 2013, MNRAS, 430, 105
Planck Collaboration, Ade, P. A. R., Aghanim, N., et al. 2016, A&A, 594, A13
Pontzen, A., & Governato, F. 2012, MNRAS, 421, 3464
Portail, M., Gerhard, O., Wegg, C., & Ness, M. 2017, MNRAS, 465, 1621
Power, C., Navarro, J. F., Jenkins, A., et al. 2003, MNRAS, 338, 14
Randall, S. W., Markevitch, M., Clowe, D., Gonzalez, A. H., & Bradač, M. 2008, ApJ, 679, 1173
Read, J. I., Agertz, O., & Collins, M. L. M. 2016, MNRAS, 459, 2573
Read, J. I., & Gilmore, G. 2005, MNRAS, 356, 107
Read, J. I., Wilkinson, M. I., Evans, N. W., Gilmore, G., & Kleyna, J. T. 2006, MNRAS, 367, 387
Reyes, R., Mandelbaum, R., Gunn, J. E., Pizagno, J., & Lackner, C. N. 2011, MNRAS, 417, 2347
Robertson, A., Massey, R., & Eke, V. 2017, MNRAS, 467, 4719
Rocha, M., Peter, A. H. G., Bullock, J. S., et al. 2013, MNRAS, 430, 81
Rodríguez-Torres, S. A., Chuang, C.-H., Prada, F., et al. 2016, MNRAS, 460, 1173
Ryden, B. S., & Gunn, J. E. 1987, ApJ, 318, 15
Salucci, P., & Burkert, A. 2000, ApJL, 537, L9
Schaller, M., Robertson, A., Massey, R., Bower, R. G., & Eke, V. R. 2015, MNRAS, 453, L58
Simon, J. D., Bolatto, A. D., Leroy, A., Blitz, L., & Gates, E. L. 2005, ApJ, 621, 757
Spekkens, K., Giovanelli, R., & Haynes, M. P. 2005, AJ, 129, 2119
Spergel, D. N., & Steinhardt, P. J. 2000, PhRvL, 84, 3760
Springel, V. 2005, MNRAS, 364, 1105
Swaters, R. A., Madore, B. F., van den Bosch, F. C., & Balcells, M. 2003, ApJ, 583, 732
Tollerud, E. J., Boylan-Kolchin, M., & Bullock, J. S. 2014, MNRAS, 440, 3511
Towns, J., Cockerill, T., Dahan, M., et al. 2014, CSE, 99, 1
Tulin, S., Yu, H.-B., & Zurek, K. M. 2013, PhRvL, 110, 111301
van der Walt, S., Colbert, S. C., & Varoquaux, G. 2011, CSE, 13, 22
Vogelsberger, M., Zavala, J., & Loeb, A. 2012, MNRAS, 423, 3740
Vogelsberger, M., Zavala, J., Simpson, C., & Jenkins, A. 2014, MNRAS, 444, 3684
Yoshida, N., Springel, V., White, S. D. M., & Tormen, G. 2000, ApJL, 544, L87
Zavala, J., Vogelsberger, M., & Walker, M. G. 2013, MNRAS, 431, L20
Zolotov, A., Brooks, A. M., Willman, B., et al. 2012, ApJ, 761, 71